Chemical Physics Letters 529 (2012) 10–15

Contents lists available at SciVerse ScienceDirect

Chemical Physics Letters

journal homepage: www.elsevier.com/locate/cplett

Ab initio calculations of autoionizing states using block diagonalization: Collinear diabatic states for dissociative recombination of electrons with N_2H^+

D.O. Kashinski [a,1], D. Talbi [b], A.P. Hickman [a,*]

[a] Department of Physics, Lehigh University, 16 Memorial Dr. East, Bethlehem, PA 18015, USA
[b] Laboratoire Univers et Particules de Montpellier, UMR 5299, CNRS and Université Montpellier II, Place Eugène Bataillon, 34095 Montpellier, France

ARTICLE INFO

Article history:
Received 13 October 2011
In final form 17 January 2012
Available online 24 January 2012

ABSTRACT

Dissociating autoionizing states for dissociative recombination of electrons with N_2H^+ have been calculated using block diagonalization. Multi-reference CI calculations for collinear N_2H and N_2H^+ were performed to assess the branching ratio to the product channels. The effects of the strong Rydberg-valence mixing in the N_2H excited states were disentangled from the changes in the molecular orbitals arising solely from N_2 bond stretching and breaking. The results suggest that $N_2 + H$ should be favored over $NH + N$, because of the absence of a favorable dissociating state for the N_2 bond breaking.

1. Introduction

Dissociative recombination (DR) [1] of electrons with molecular ions occurs in planetary atmospheres, in the interstellar medium, and in tokamak plasmas. Calculating appropriate potential curves to treat this process is difficult because the states involved are autoionizing, that is, they are embedded in a continuum of electron–ion scattering states. In previous work on HCNH [2], we showed that the potential curves describing HN and HC bond breaking could be viewed as diabatic states and calculated using the block diagonalization method [3–5]. In this Letter we consider a more complex situation in which either the strong N_2 bond or the NH bond may be broken.

Although nitrogen is very important in the chemistry of the interstellar medium, it cannot be directly observed. Its abundance must be inferred indirectly by detecting N_2H^+, which can be produced by the reaction

$$N_2 + H_3^+ \rightarrow N_2H^+ + H_2 \quad (1)$$

It was long assumed that the N_2 consumed in reaction (1) was almost completely recovered by DR. The measurements of Adams et al. [6] in 1990 indicated that the branching ratios in the DR process strongly favor the $N_2 + H$ channel:

$$e^- + N_2H^+ \rightarrow \begin{cases} N_2 + H \\ NH + N \end{cases} \quad (2)$$

However, in 2004 Geppert et al. [7] reported measurements that the branching ratio to the $NH + N$ channel was dominant. This unexpected result cast doubt on the assumptions mentioned above and motivated additional experimental and theoretical work.

In 2007, Molek et al. [8] reported a new experimental measurement of the branching ratio and concluded that the upper limit for the branching ratio to the $NH + N$ channel was 5%. Also in 2007, Talbi [9] reported a theoretical investigation of the potential surfaces for linear N_2H and N_2H^+. By considering quasi-diabatic states determined by an approximate method from her high-level structure calculations, she concluded that the most likely outcome of dissociative recombination would be the $N_2 + H$ channel, with N_2 in the first electronically excited state. There is now general agreement that the branching ratio to the $NH + N$ channel is less than about 5% [1].

Talbi's work [9,10] highlighted the need for electronic structure calculations that could implement a systematic methodology for determining the autoionizing states of N_2H, especially for short NH or NN bond lengths. A preliminary report [11] of some of our work along these lines has appeared. For DR processes, potential surfaces are needed for the initial molecular ion, the Rydberg states of the corresponding neutral, and the dissociating autoionizing state. These surfaces are illustrated schematically in Figure 1. Calculating the potential surface for the initial molecular ion or for the Rydberg states requires only standard techniques of quantum chemistry. Calculating the dissociating state is much more difficult, because that state is embedded in the continuum of scattering states ($e^- + N_2H^+$ in the present case). In practice, the states of interest are highly excited and strongly mixed with other states. Multiple curve crossings occur, and isolating the desired potential surfaces can be very difficult. Recent work by ourselves [2,12] and others [3–5] has shown that the block diagonalization method

* Corresponding author. Fax: +1 610 758 5730.
E-mail addresses: dkashinski@gmail.com (D.O. Kashinski), dahbia.talbi@univ-montp2.fr (D. Talbi), aph2@lehigh.edu (A.P. Hickman).
[1] Current address: Department of Physics & Nuclear Engineering, United States Military Academy, West Point, NY 10996, USA.

0009-2614/$ - see front matter © 2012 Elsevier B.V. All rights reserved.
doi:10.1016/j.cplett.2012.01.037

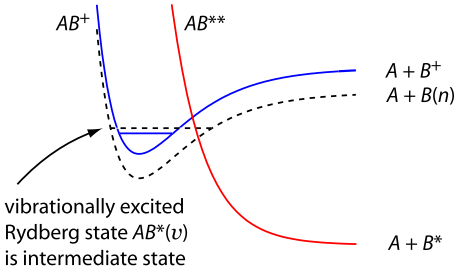

Figure 1. Potential curves for the molecular ion and the dissociating neutral state needed for DR. A representative Rydberg curve is shown by the dashed line.

provides a very powerful technique to determine the necessary dissociating, autoionizing states of N_2H.

The present work presents calculations of collinear electronic potential energy surfaces and coupling terms for DR of electrons with N_2H^+. Section 2 provides a brief summary of the block diagonalization method. Section 3 describes the electronic structure calculations we performed and includes a discussion of the special techniques we implemented. Section 4 describes the determination of the diabatic potential surfaces.

2. Block diagonalization method

Our electronic structure calculations of the resonant autoionizing states rely on the block diagonalization method, so we briefly describe that procedure here. The block diagonalization method [3,4] provides an effective technique for transforming the results of a standard electronic structure calculation into diabatic potential curves.

Care must be taken in the determination of molecular orbitals (MOs) ϕ_i so that their variation with molecular geometry is smooth. In previous work [2], we followed [3] and took advantage of the fact that the energies of a Multi-Configuration Self-Consistent Field (MCSCF) calculation are invariant under an arbitrary rotation **U** of the MOs in the active space [13,14], and we implemented a rotation of the MCSCF orbitals that made each MO resemble as closely as possible a corresponding orbital in a set of 'reference' orbitals that were determined in the separated atom limit. In the present work a simpler approach was possible. The core and valence MOs were taken to be the natural orbitals determined in a CI (configuration interaction) calculation of the ground state electronic wave function for the neutral molecule, and the Rydberg MOs were determined separately in a smaller, frozen-core calculation.

The CI electronic wave function Ψ_n for the nth state is represented as the sum of CSFs (configuration state functions) Φ_m, each constructed from the MOs ϕ_i:

$$\Psi_n = \sum_{m=1}^{N} c_{nm}\Phi_m \tag{3}$$

The number of coefficients N in the sum in Eq. (3) may be quite large (of order 10^6). However, one can usually identify a small set of N_α configurations ($N_\alpha \sim 2$—10) that make the dominant contribution to N_α electronic states of interest. Then N_α will be the dimension of the diabatic Hamiltonian, and for the diabatization one only needs the $N_\alpha \times N_\alpha$ matrix of values c_{mn} for the coefficients of the N_α dominant configurations in the N_α states of interest. We denote this matrix by **S**. The diabatic Hamiltonian matrix $\mathbf{H}_{\rm dia}$ can be expressed as a transformation of the diagonal matrix **E** whose nonzero elements are the adiabatic eigenvalues $E_1, \ldots, E_{N_\alpha}$:

$$\mathbf{H}_{\rm dia} = \mathbf{T}^\dagger\mathbf{E}\mathbf{T} \tag{4}$$

where (†) denotes the adjoint (transpose for a real transformation), and

$$\mathbf{T} = \mathbf{S}^{-1}\left(\mathbf{S}\mathbf{S}^\dagger\right)^{1/2} \tag{5}$$

In many cases certain linear combinations of CSFs appear repeatedly in the wave functions described by Eq. (3). For example, certain pairs of CSFs (say Φ_p and Φ_q) often appear with nearly the same coefficient, or with coefficients of similar magnitude but opposite sign. Then a transformation to 'super-CSFs' $(\Phi_p \pm \Phi_q)/\sqrt{2}$ is advantageous, because a state of interest may then be dominated by a single super-CSF, leading to a smaller number of super-CSFs needed. We describe later the use of super-CSF with up to four CSFs; the transformation to the alternate CSFs can be easily formulated as a basis set transformation of the eigenvectors of the CI.

This analysis of the adiabatic eigenvalues and eigenvectors, including the transformation to super-CSFs, is done after the GAMESS calculation is completed, using a separate computer code that we wrote. The calculations are straightforward and only involves matrices of dimension N_α. Since $\mathbf{H}_{\rm dia}$ is explicitly constructed by a unitary transformation of the matrix **E** of adiabatic eigenvalues, the eigenvalues of the small matrix $\mathbf{H}_{\rm dia}$ will be exactly the same as the chosen N_α eigenvalues of the large matrix determined by the CI calculation. This point should be emphasized: the eigenvalues of the final, diabatic potential matrix $\mathbf{H}_{\rm dia}$ determined using Eqs. (4) and (5) correspond *exactly* to the adiabatic energies that we obtain in the CI. The diabatization does not compromise the quantum chemistry. It requires that we take a few extra steps in the structure calculations, but it does not degrade the results.

3. Electronic structure calculations

3.1. General remarks

The electronic structure calculations reported here were performed using the GAMESS code [15]. We used the basis set specified by Talbi [9]: a 6-311G(d,p) on each N plus diffuse functions and a 10*s*4*p*1*d* basis on H. There were 69 total basis functions. Using the notation of Talbi [9] for the molecular orbitals, the orbital occupancy of the ground state of N_2H^+ is

$$1s_a^2\,1s_b^2\,(\mathrm{NN})^2(\mathrm{SP})^2(\mathrm{NH})^2\,\pi_x^2\pi_y^2 \tag{6}$$

DR involves the capture of an electron into a virtual orbital, leading to the formation of a linear excited state of the parent neutral molecule. If the virtual orbital is the anti-bonding NH*, the resulting electronic configuration will be

$$1s_a^2 1s_b^2(\mathrm{NN})^2(\mathrm{SP})^2(\mathrm{NH})^2\pi_x^2\pi_y^2(\mathrm{NH}^*)^1 \tag{7}$$

for which the NH bond is weakened. The configuration above is the lowest of those available for the DR of N_2H^+ and leads to the products $N_2 + H$ in their ground electronic states. The lowest configuration leading to dissociation into the products $\mathrm{NH}(X^3\Sigma^-) + \mathrm{N}(^2D)$ is a linear combination of CSFs corresponding to the following two orbital occupancies:

$$1s_a^2 1s_b^2(\mathrm{NN})^2(\mathrm{SP})^2(\mathrm{NH})^2\pi_x^0\pi_y^2(\mathrm{NH}^*)^1\pi_x^{*1}\pi_y^{*1} \tag{8}$$

$$1s_a^2 1s_b^2(\mathrm{NN})^2(\mathrm{SP})^2(\mathrm{NH})^2\pi_x^2\pi_y^0(\mathrm{NH}^*)^1\pi_x^{*1}\pi_y^{*1} \tag{9}$$

The Rydberg states of N_2H have one electron in a highly excited orbital outside of the ion core:

$$1s_a^2 1s_b^2(\mathrm{NN})^2(\mathrm{SP})^2(\mathrm{NH})^2\pi_x^2\pi_y^2(\mathrm{NH}^*)^0(\pi_x^*)^0(\pi_y^*)^0$$
$$(\mathrm{NN}^*)^0(\mathrm{Ryd1})^1(\mathrm{Ryd2})^0(\mathrm{Ryd3})^0\ldots \tag{10}$$

For a quantitative study of DR of N_2H^+ that includes both the $N_2 + H$ and $NH + N$ reaction channels, an even-handed treatment of the ionic states, the excited states (mainly Rydbergs), and the dissociative states of linear N_2H is required. Correlation energies must be

Table 1
Summary of the different orbital active spaces used for the differing levels of calculation.

MCSCF; FOCI-1 for ground state	$(SP)(NN)(NH)(\pi_x)(\pi_y)(NH^*)(\pi_x^*)(\pi_y^*)(NN^*)$
Final FOCI	$(SP)(NN)(NH)(\pi_x)(\pi_y)(NH^*)$ $(\pi_x^*)(\pi_y^*)(NN^*)$(Ryd 1)(Ryd 2)(Ryd 3)

treated through the same CI procedure so as not to favor one state over another. This requirement holds for all states that might be involved in the recombination of the ion and all along the two dissociative reaction coordinates.

To satisfy these requirements we have completed first order configuration interaction (FOCI) calculations (CI with single excitations) using the final active space given in Table 1. The $(1s_a)$ and $(1s_b)$ orbitals are treated as a frozen core. The calculations included a total of 5,788,144 CSFs; comparison with estimated vertical excitation energies of N_2 from reference [16] showed an accuracy of about 0.1 eV. We typically calculated 15–20 eigenvalues and eigenvectors of the electronic Hamiltonian.

3.2. Calculations for N_2H

Potential energy curves were calculated for N_2H as a function of the NH bond length R_{NH}, with the NN bond distance R_{NN} fixed at the N_2H^+ equilibrium value of 1.12 Å, and as a function of the bond length R_{NN}, with the NH bond distance fixed at the N_2H^+ equilibrium value of 1.05 Å [9,10]. These geometries were chosen because the initial conditions for dissociative recombination are determined by the ion's geometry. The NN or NH bond lengths in the possible fragments are very close to their values in the initial ion, so we do not expect a large change in the PES by fixing one of the distances when the other is varied toward dissociation. We verified that point in our previous studies of DR of electrons with HCO^+ [17]. Adiabatic and diabatic potential energy curves for several electronic states were determined. In most respects the calculations follow established procedures for performing MRCI calculations; however, some additional work was involved in the determination of suitable MO's. We now describe how the MO's were determined.

3.2.1. MCSCF calculations

The first major step of generating MO's was an MCSCF calculation. For linear N_2H the occupancy of the lowest electronic state was

$$1s_a^2 1s_b^2 (NN)^2 (SP)^2 (NH)^2 \pi_x^2 \pi_y^2 (NH^*)^1 \tag{11}$$

We performed a single-state MCSCF and then an FOCI calculation, denoted FOCI-1, for the electronic ground state. The active space for these calculations is specified in Table 1. Both calculations assumed the C_{2v} point group for the molecule and were restricted to electronic states of A_1 symmetry. The natural orbitals from FOCI-1 were very well behaved. We performed the final, multi-root FOCI calculation using a set of orbitals formed by combining these FOCI-1 natural orbitals with selected Rydberg orbitals calculated as described below in Section 3.2.2.

3.2.2. Rydberg orbitals

The last step in calculating the MO's was to determine a set of well-defined Rydberg orbitals. Many of the diabatic states that we calculate correspond to a core N_2H^+ ion plus a single, highly-excited electron. Being able to describe these states by a single CSF simplifies the block diagonalization process and facilitates the analysis of Rydberg-valence coupling.

Using orbitals generated for the ion at the SCF level, we performed a single CI calculation in A_1 symmetry for N_2H with seven doubly occupied frozen core orbitals and one electron in the remaining orbitals. This CI provides a well defined set of orbitals: the first seven comprise the frozen core of N_2H^+ from the RHF-SCF calculation, the next orbital is identified as NH*, and then there are several orbitals of Rydberg character. In our final FOCI calculation, we substitute these Rydberg orbitals for the A_1 natural orbitals obtained in the N_2H FOCI-1. Then the electronic Rydberg states have the form of a N_2H^+ core and an excited electron in a single, easily identified orbital:

$$1s_a^2 1s_b^2 (NN)^2 (SP)^2 (NH)^2 \pi_x^2 \pi_y^2 (NH^*)^0 (\pi_x^*)^0 (\pi_y^*)^0 (NN^*)^0 (Rydn)^1 \quad n = 1, \ldots, 8 \tag{12}$$

Swapping the orbitals as described above is justified because the Rydberg orbitals from the frozen core calculation span almost exactly the same space as the virtual space orbitals determined by FOCI-1. We confirmed this fact by explicitly rotating all of the virtual FOCI-1 natural orbitals (NOs) so that they were aligned with the Rydberg orbitals from the frozen core, single CI calculations. After the rotation, corresponding pairs of orbitals exhibited very high overlap (inner products around 0.9999), confirming that the Rydberg orbitals are simply related to the FOCI-1 NOs by a rotation and are not a fundamentally different basis set. It is known that such a rotation in the active space will not change the adiabatic energies of a CAS-MCSCF (Complete Active Space MCSCF) calculation [13,14].

The replacement just described only works for values of $R_{NH} \leqslant 2.30$ Å. The method breaks down for larger R_{NH} because then the core cannot be treated as a single entity but as N_2^+ and H. For large R_{NH} the Rydberg-like states are very high and no longer interact with the dissociating state of interest, and it was sufficient simply to use the Rydberg orbitals generated at $R_{NH} = 2.30$ Å. This approach provided a smooth transition to geometries with very large R_{NH}. We did not need to make this adjustment for the calculations as a function of R_{NN}, because we did not extend the calculations to large R_{NN}.

3.3. Calculations for N_2H^+

We performed calculations for N_2H^+ at the same geometries used for N_2H. These calculations were very standard. We used the same orbitals and active space that we used for the final FOCI on N_2H, and there were 998,760 CSFs. Obtaining a surface for the ground state of N_2H^+ required no further processing after the GAMESS calculation.

4. Determination of diabatic potential curves

The ideal situation for the block diagonalization method described in Section 2 is where one can easily identify a set of N_α CSFs that make the dominant contributions to N_α eigenvectors of the electronic Hamiltonian. In our calculations for N_2H the situation was not always clear cut, because the set of important CSFs depended on the geometry of the molecule. As one changed the coordinates of the nuclei, certain CSFs might become more or less important, leading to uncertainties about how to achieve a consistent treatment. Part of this phenomena is due to the strong coupling between Rydberg and valence configurations in the wave function. Another part, however, arises solely from the changes in the MOs that accompany breaking of the N_2 bond. If one is to treat a DR process that involves dissociation by breaking an N_2 bond, then one must be able to separate out the expected bond-breaking behavior from the effects due to the Rydberg-valence coupling. An effective way to separate these two effects was to

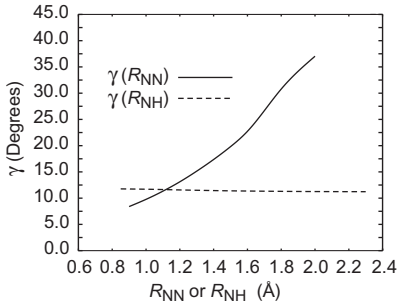

Figure 2. The mixing angle γ in the GVB approximation determined from Eq. (15) as a function of R_{NN} (for $R_{NH} = 1.05$ Å) and of R_{NH} (for $R_{NN} = 1.12$ Å).

define a geometry-dependent super-CSF that mimicked the two-component generalized valence bond (GVB) wavefunction for treating strong covalent bonds. This section describes how we implemented this method.

4.1. The GVB super-CSF

Section 2 mentioned that we could often identify certain linear combinations of CSFs (called super-CSFs) that frequently appeared in the eigenvectors. A super-CSF can be defined that corresponds to the GVB wave function for N_2H, thereby providing a chemically reasonable approximation to N_2H for the entire range of N_2 bond lengths.

The GVB wave function for two electrons may be expressed in a form compatible with GAMESS [18] by using a pair of orthogonal orbitals ϕ_g and ϕ_u:

$$\Psi_{GVB}(1,2) = \cos\gamma|\phi_g\overline{\phi}_g\rangle - \sin\gamma|\phi_u\overline{\phi}_g\rangle \tag{13}$$

where ϕ_g and ϕ_u are symmetric and antisymmetric combinations of two identical orbitals on the left and the right atomic center (the left and right N in the present case); $|\phi_g\overline{\phi}_g\rangle$ and $|\phi_u\overline{\phi}_g\rangle$ denote Slater determinants; the overbar denotes spin down, and γ is a mixing angle related to the electron density defined by

$$\rho(1) = 2\int |\Psi_{GVB}(1,2)|^2 d2 = 2\phi_g^2\cos^2\gamma + 2\phi_u^2\sin^2\gamma \tag{14}$$

The value of γ can be easily determined from the density matrix determined by GAMESS. The final molecular orbitals always included a pair that could be identified as ϕ_g and ϕ_u, so the corresponding coefficients ρ_{gg} and ρ_{uu} in the density matrix correspond to $2\cos^2\gamma$ and $2\sin^2\gamma$, respectively. Specifically, we determine γ from

$$\tan^2\gamma = \rho_{uu}/\rho_{gg} \tag{15}$$

γ varies from 0 in the pure covalent limit to 45° in the separated atom limit. For the values of R_{NN} we considered, γ does not reach either limit. The calculated values are shown in Figure 2.

In the case of N_2H there are two π orbitals, π_x and π_y, as well as two π^* orbitals, π_x^* and π_y^*. We treat the x and y orbitals both with a single GVB wave function and then take the antisymmetric product to produce the approximate GVB wave function for the π orbitals of the molecule:

$$\begin{aligned}\Psi_{GVB}^{xy} &= \mathcal{A}\Psi_{GVB}^{x}\Psi_{GVB}^{y}\\ &= \left(\cos\gamma|\phi_g^x\overline{\phi}_g^x\rangle - \sin\gamma|\phi_g^x\overline{\phi}_g^x\rangle\right)\\ &\quad\times\left(\cos\gamma|\phi_g^y\overline{\phi}_g^y\rangle - \sin\gamma|\phi_u^y\overline{\phi}_u^y\rangle\right)\end{aligned} \tag{16}$$

We can identify the CSFs for N_2H that correspond to electronic states with the π_x and π_y electrons in the orbitals given in Eq. (16) and with the other electrons in the appropriate orbitals for the dissociating state. We can then write the expression for Φ_{GVB} as the definition of a super-CSF for N_2H:

$$\begin{aligned}\Phi_{GVB} = \cos^2\gamma|\ldots\phi_g^x\overline{\phi}_g^x\phi_g^y\overline{\phi}_g^y\ldots\rangle &+ \sin^2\gamma|\ldots\phi_u^x\overline{\phi}_u^x\phi_u^y\overline{\phi}_u^y\ldots\rangle\\ &- \sin\gamma\cos\gamma|\ldots\phi_g^x\overline{\phi}_g^x\phi_u^y\overline{\phi}_u^y\ldots\rangle\\ &- \sin\gamma\cos\gamma|\ldots\phi_u^x\overline{\phi}_u^x\phi_g^y\overline{\phi}_g^y\ldots\rangle\end{aligned} \tag{17}$$

This expression for Φ_{GVB} allows us to identify the CSFs in our large GAMESS calculation that correspond to those that are involved in the GVB approximation. We can use Eq. (17) to define a super-CSF with four CSFs whose coefficients depend on geometry through γ [which is calculated using Eq. (15)]. This super-CSF is essentially the GVB approximation to the wave function.

4.2. Diabatic potential curves for both dissociating channels

The careful choice of MOs and the use of the super-CSFs enabled us to identify a total of $N_\alpha = 6$ CSFs that made the dominant contribution to the lowest six eigenvectors. We then carried out the block diagonalization procedure to obtain slices of the collinear potential surface for the two possible dissociation channels.

The results confirm that the GVB super-CSF provides a compact description of the behavior of the NN bond. For several values of R_{NN}, Table 2 shows the coefficients of the original CSFs that comprise Φ_{GVB} [cf. Eq. (17)]. These coefficients are calculated by GAMESS in the matrix diagonalization. The table also shows the inner product $\langle\Phi_{GVB}|\Psi_G\rangle$, which corresponds to the projection of the full GAMESS CI wave function onto the single basis vector Φ_{GVB}. One can see that as the NN bond stretches, the super-CSF accounts for a significantly larger portion of the full wave function than the single CSF corresponding to a double NN bond. We therefore expect a more reliable diabatic representation.

We also applied the full GVB analysis to the $N_2 + H$ channel, but we found that using Φ_{GVB} was not necessary when R_{NN} was near its equilibrium value. That result is not surprising; in that case γ is small, and the coefficients in Eq. (17) show that $\cos^2\gamma \approx 1$, and Φ_{GVB} is dominated by the CSF corresponding to the double NN

Table 2
Coefficients of the CSFs in the super-CSF Φ_{GVB} [given by Eq. (17)] and in the GAMESS wave function Ψ_G, for several values of R_{NN}. R_{NH} is fixed at 1.050 Å. The inner product $\langle\Phi_{GVB}|\Psi_G\rangle$ is significantly larger than the coefficient of Ψ_G corresponding to the CSF $|\ldots\phi_g^x\overline{\phi}_g^x\phi_g^y\overline{\phi}_g^y\ldots\rangle$; this difference indicates that the single super-CSF Φ_{GVB} includes more of the bond-breaking behavior contained in Ψ_G.

CSF Φ	$R_{NN} = 1.120$ Å, $\gamma = 11.67°$ Coefficient of Φ		$R_{NN} = 1.600$ Å, $\gamma = 22.73°$ Coefficient of Φ		$R_{NN} = 1.800$ Å, $\gamma = 30.79°$ Coefficient of Φ	
	in Φ_{GVB}	in Ψ_G	in Φ_{GVB}	in Ψ_G	in Φ_{GVB}	in Ψ_G
$\|\ldots\phi_g^x\overline{\phi}_g^x\phi_g^y\overline{\phi}_g^y\ldots\rangle$	0.959061	0.938802	0.850710	0.815490	0.738024	0.679547
$\|\ldots\phi_u^x\overline{\phi}_u^x\phi_u^y\overline{\phi}_u^y\ldots\rangle$	0.040938	0.034044	0.149290	0.125980	0.261976	0.196674
$\|\ldots\phi_g^x\overline{\phi}_g^x\phi_u^y\overline{\phi}_u^y\ldots\rangle$	−0.198148	−0.132706	−0.356374	−0.264421	−0.439710	−0.323727
$\|\ldots\phi_u^x\overline{\phi}_u^x\phi_g^y\overline{\phi}_g^y\ldots\rangle$	−0.198148	−0.137706	−0.356374	−0.264421	−0.439710	−0.323727
	$\langle\Phi_{GVB}\|\Psi_G\rangle = 0.95798$		$\langle\Phi_{GVB}\|\Psi_G\rangle = 0.90109$		$\langle\Phi_{GVB}\|\Psi_G\rangle = 0.83774$	

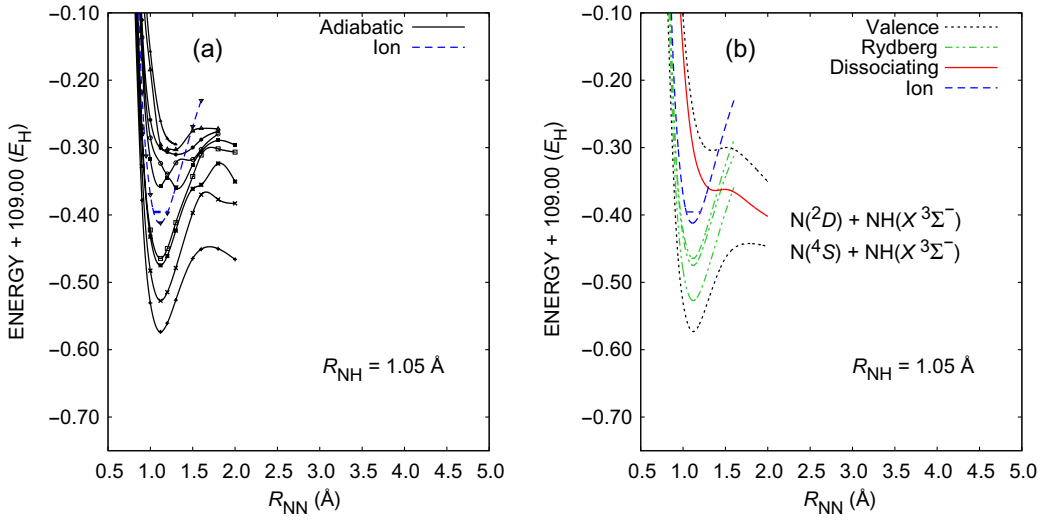

Figure 3. Panel (a) shows the first 10 adiabatic roots of N_2H as a function of R_{NN} for the linear molecule, and panel (b) shows the corresponding diabatic curves. The dashed curve represents the ground state of the ion. The solid curve is the dissociative state of interest.

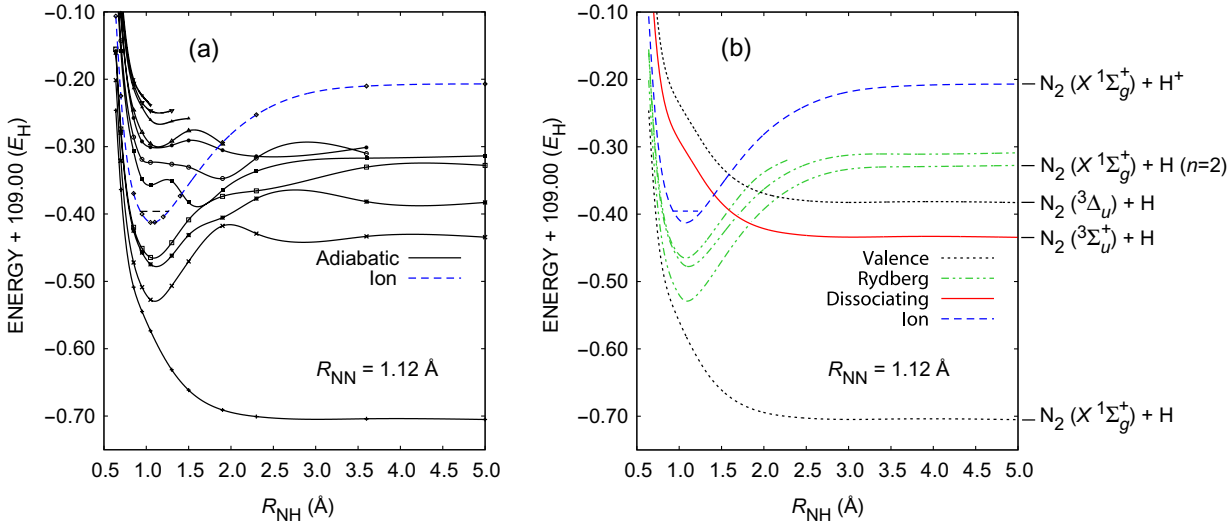

Figure 4. Panel (a) shows the first 10 adiabatic roots of N_2H as a function of R_{NH} for the linear molecule, and panel (b) shows the corresponding diabatic curves. The dashed curve represents the ground state of the ion. The solid curve is the dissociative state of interest.

bond. Figure 2 shows that γ is small and slowly varying as a function of R_{NH}.

Figure 3 shows the adiabatic and diabatic potential curves as a function of R_{NN}, with R_{NH} fixed at its equilibrium value in N_2H^+. Figure 4 shows similar curves as a function of R_{NH}, with R_{NN} fixed at its equilibrium value in N_2H^+. From these curves one can assess the effectiveness of the 'direct mechanism' for DR by considering the overlap (or Franck–Condon factor) between the initial vibrational wave function of the molecular ion and the continuum wave function of the final scattering state (at the same total energy). For a large overlap the diabatic dissociating state should cross the ion potential between the classical turning points for the initial vibrational motion. The dissociating curves in Figs. 3b and 4b are qualitatively very similar to those estimated by Talbi [9] and support her conclusion that the most likely products of dissociative recombination are $N_2 + H$. The crossings for both dissociating channels are unfavorable and suggest that the direct mechanism of DR will not be effective. The indirect mechanism or the Renner–Teller effect may play a role for the $N_2 + H$ channel, just as they do for the case of HCO [19,20]. However, the plateau-like feature of the dissociating curve leading to $NH + N$ in Figure 3b is so wide that it appears unlikely to provide an exit channel for an indirect process involving a vibrationally excited Rydberg level.

5. Concluding remarks

We have completed large scale electronic structure calculations for the ground state of N_2H^+ and for several states of N_2H, including the dissociating state important for dissociative recombination. The powerful technique of block diagonalization allows us to determine these diabatic, autoionizing states using methodology that can easily implemented in standard electronic codes such as GAMESS. The present techniques will be extended to treat bent geometries of N_2H, which are needed for a definitive investigation of the dynamics. Further work is also planned to address other DR processes in which multiple dissociation channels are available.

Acknowledgements

D.O.K. and A.P.H. acknowledge support from National Science Foundation Grant No. PHY-0652938. D.T. acknowledges support

from the French national PCMI program. Computational facilities at NCSA and PSC used for this research were supported by the National Science Foundation through XSEDE resources provided by the XSEDE Science Gateways program.

References

[1] M. Larsson, A. Orel, Dissociative Recombination of Molecular Ions, Cambridge University Press, New York, 2008.
[2] A.P. Hickman, R.D. Miles, C. Hayden, D. Talbi, Astron. Astrophys. 438 (2005) 31.
[3] T. Pacher, L.S. Cederbaum, H. Köppel, J. Chem. Phys. 89 (1988) 7367.
[4] W. Domcke, C. Woywod, Chem. Phys. Lett. 216 (1993) 362.
[5] L.S. Cederbaum, J. Schirmer, H.-D. Meyer, J. Phys. A: Math. Gen. 22 (1989) 2427.
[6] N.G. Adams et al., J. Chem. Phys. 34 (1991) 4852.
[7] W.D. Geppert et al., Ap. J. 609 (2004) 459.
[8] C.D. Molek, J.L. McLain, V. Poterya, N.G. Adams, Phys. Rev. A 29 (2007) 1548.
[9] D. Talbi, Chem. Phys. 332 (2007) 298.
[10] D. Talbi, J. Phys. Conf. Ser. 192 (2009) 012015.
[11] A.P. Hickman, D.O. Kashinski, R.F. Malenda, F. Gatti, D. Talbi, J. Phys. Conf. Ser. 300 (2011) 012016. 8 pages.
[12] J.A. Spirko, J.T. Mallis, A.P. Hickman, J. Phys. B: At. Mol. Opt. Phys 33 (2000) 2395.
[13] B.O. Roos, Adv. Chem. Phys. 69 (1987) 399.
[14] M.W. Schmidt, M.S. Gordon, Ann. Rev. Phys. Chem. 49 (1998) 233.
[15] M.W. Schmidt et al., J. Comp. Chem. 14 (1993) 1347.
[16] F.R. Gilmore, J. Quant. Spect. Radiat. Trans. 5 (1965) 369.
[17] D. Talbi, A.P. Hickman, F. Pauzat, Y. Ellinger, G. Berthier, Ap. J 339 (1989) 231.
[18] A. Szabo, N.S. Ostlund, Modern Quantum Chemistry: Introduction to Advanced Electronic Structure Theory, Macmillan, Publishing Co., Inc., New York, 1982.
[19] I.A. Milhailov, V. Kokoouline, A. Larson, S. Tonzani, C.H. Greene, Phys. Rev. A 74 (2006) 032707 (9 pages).
[20] C. Jungen, S.T. Pratt, J. Chem. Phys. 129 (2008) 164311 (9 pages).